

Experimental investigation of the transverse resistivity in Nb₃Sn wires through ac susceptibility

This content has been downloaded from IOPscience. Please scroll down to see the full text.

2013 Supercond. Sci. Technol. 26 085001

(<http://iopscience.iop.org/0953-2048/26/8/085001>)

View [the table of contents for this issue](#), or go to the [journal homepage](#) for more

Download details:

IP Address: 188.184.64.214

This content was downloaded on 17/06/2015 at 14:59

Please note that [terms and conditions apply](#).

Experimental investigation of the transverse resistivity in Nb₃Sn wires through ac susceptibility

P Fabbricatore¹, S Farinon¹, V Corato², G De Marzi², T Spina²,
U Gambardella³ and A Saggese⁴

¹ INFN-Sezione di Genova, Via Dodecaneso, 33, I-16146 Genova, Italy

² ENEA Frascati, Via E Fermi, 65, I-00044 Frascati, Italy

³ INFN-Sezione di Napoli, Via Cintia, I-80126 Napoli, Italy

⁴ CNR-SPIN, UOS Salerno, Dipartimento di Fisica, Università di Salerno, I-84084 Fisciano, Italy

E-mail: umberto.gambardella@sa.infn.it

Received 18 March 2013, in final form 14 May 2013

Published 10 June 2013

Online at stacks.iop.org/SUST/26/085001

Abstract

In this paper we compare two different experimental methods to estimate the transverse resistivity in superconducting NbTi and Nb₃Sn multifilament wires. The first method is based on direct measurements of the resistance through micro wires bonded on the cross section of the strand. The second method exploits the physical meaning of the ac susceptibility of the multifilament wires. Both methods have been previously used: the first on Nb₃Sn and NbTi strands, while the second has been applied only to NbTi wires. Here we first compare and analyze results in a NbTi system, then we extend the ac susceptibility method to Nb₃Sn wires. The advantages and the limits of both techniques, when used on wires with different layouts, are analyzed. The results of the transverse resistivity obtained by using the two experimental methods are finally compared to the estimation based on a numerical approach.

(Some figures may appear in colour only in the online journal)

1. Introduction

In a superconducting (s/c) multifilament wire exposed to an ac transverse magnetic field the coupling currents between filaments represent a relevant loss in addition to the intrinsic hysteresis losses of the superconducting filaments. Thus knowledge of the losses caused by the eddy currents crossing the normal conducting matrix is of crucial importance in keeping the overall losses within stringent values. There are two main design parameters affecting the coupling losses in a multifilament wire: the twist pitch L of the filaments and the transverse resistivity ρ_{et} , representing the overall resistivity of the matrix with respect to the current loops among filaments flowing through the normal conducting matrix [1]. This last quantity also determines the current redistribution length among different filaments, which is an important parameter when the critical current density J_c is locally affected by bending strain in the Nb₃Sn wires.

In the past, different experimental methods for measuring the ac losses in a multifilament s/c wire have been developed, based on self-field distribution [2], magnetization [3] and current transfer length [4] measurements. Here we limit our attention to new experimental techniques, based on the ac susceptibility [5] or on the dc resistance measurement [6–8], to measure ρ_{et} in multifilament wires. The ac technique has been previously applied only to a NbTi thin filament strand used into the fast cycled superconducting dipoles for the SIS300 synchrotron at FAIR [9], where the magnetic field is fast ramped at 1 T s^{-1} . The dc technique has been used instead on Nb₃Sn and NbTi wires for nuclear fusion applications, e.g. the Central Solenoid or the Toroidal Field magnets in the ITER or JT60-SA projects [10, 11]. In the first case a model to measure the characteristic frequency f_0 (i.e. $1/\tau$, with τ being the characteristic current decay time in a s/c multifilament wire) in a multifilament wire has been developed, from which ρ_{et} can be straightforwardly derived.

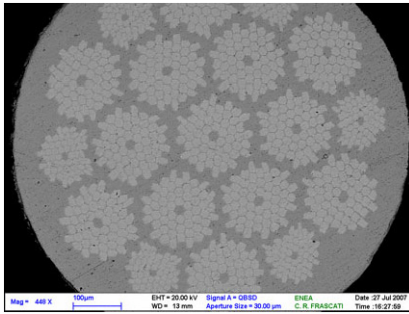


Figure 1. SEM image of the JT60-SA NbTi wire cross section.

In the second case a direct four-point contact measurement of the resistance between filament bundles is performed. Both techniques have been supported by numerical models [5, 12] that substantially confirm the results obtained.

In this paper we firstly verified the agreement of the results obtained by dc resistance and ac susceptibility techniques in a NbTi sample, then we extended the comparison to Nb₃Sn wires used for fusion applications. The aim of the work is to explore the advantages and the limits of the ac susceptibility method in the Nb₃Sn system: it is contactless, less time consuming, and allows a global estimate of ρ_{et} regardless of the strand layout, but it cannot be applied to any configuration.

In section 2 we summarize the conditions we used in performing the experiments in both kinds of wires. In section 2.1 we examine a NbTi wire, labeled JT60-SA, analyzing first the dc resistive measurement and its relation to the ρ_{et} . Then we present the results obtained through ac susceptibility measurements on the same wire. In section 2.2 we analyze several Nb₃Sn wire layouts, and the ac and dc results, showing some limits in Nb₃Sn ac susceptibility measurements. In section 3 we discuss the key points related to these different approaches and compare the experimental values to the results of numerical simulations. Conclusions are finally drawn in section 4.

2. Wires and measurements

In this section we report the experiments performed on the *s/c* strands used in cables for fusion programs, whose features are widely reported in the literature.

2.1. NbTi wire

The multifilament NbTi wire was designed for the fusion device JT60-SA, and manufactured by Luvata (Italy) [13]. The NbTi strand (0.81 mm in diameter) is made of 19 filament bundles embedded in a Cu matrix, each bundle being formed by 54 filaments having a diameter of 20 μm . Its Cu:non-Cu ratio is equal to 1.86. The wire cross section is shown in figure 1. The transverse resistance R_t between different bundles has been measured through thin Al wires, about 25 μm in diameter, ultrasonically bonded on the sub-elements. The four-point voltage–current curves have been collected by injecting the current in a couple of sub-elements, and measuring the voltage at increasing

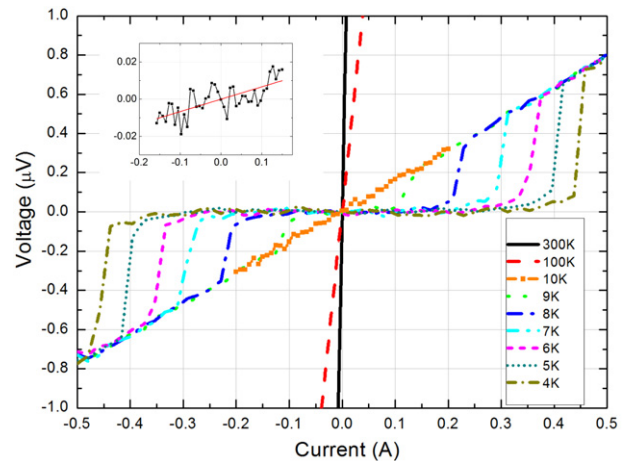


Figure 2. Voltage–current characteristics measured on the JT60-SA wire, $h = 0.94$, with a four-probe technique on the wire cross section. A zoom of the zero-bias region is reported in the inset.

current from the other two signal wires on the same two sub-elements, but in different locations. The measurements have been performed in a ⁴He gas flow cryostat, with the sample shielded from the direct cooling He gas flow by means of a copper box. Details of the experimental setup are discussed in [6]. In order to understand the current distribution through the section of the NbTi strand, R_t between different bundles has been estimated on samples having different lengths, h : $h_1 = 0.94$ mm, $h_2 = 1.62$ mm, $h_3 = 2.75$ mm. The voltage–current characteristics have been measured for different temperatures in the range 4.2–300 K, as shown in figure 2. At temperatures above the critical temperature, T_c , the curves are linear, because of the Ohmic behavior of the strand, and the resistance value R_t is obtained through a linear fit, whereas for $T < T_c$ the superconducting transition causes non-linear characteristics. In this situation, $R_t(T)$ is obtained by fitting the linear part of the curves, around the zero bias, as shown in the inset of figure 2. For $T < T_c$ the dependence of the resistance on $1/h$ is linear, as foreseen in [12], whereas R_t is independent of the sample length for $T > T_c$. From a physical point of view the current distribution is expected to occur along the whole sample length below T_c and within a negligible length above T_c .

Thus, once R_t has been determined, the corresponding effective resistivity in the superconducting state can be derived by the simple formula [7]: $\rho_{et}^{el} = hR_t$, where h is the sample length. To attain a comparable condition with the ac experiments, performed in a transverse static magnetic field of 0.2 T, the R_t was measured also by applying 0.2 T, but with the magnetic field direction parallel to the filaments. In this condition we obtain $\rho_{et}^{el} = (0.09 \pm 0.03)$ n Ω m.

The inductive measurements, aimed at the determination of the dynamical effective resistivity, ρ_{et}^{mag} , were carried out on a coil-shaped NbTi sample of the same wire tested with the electrical technique. Since the characteristic frequency f_0 depends on the filament twist pitch, the length of the sample was selected in order to be longer than one twist pitch. In the ac technique, the in-phase and out-of-phase signals

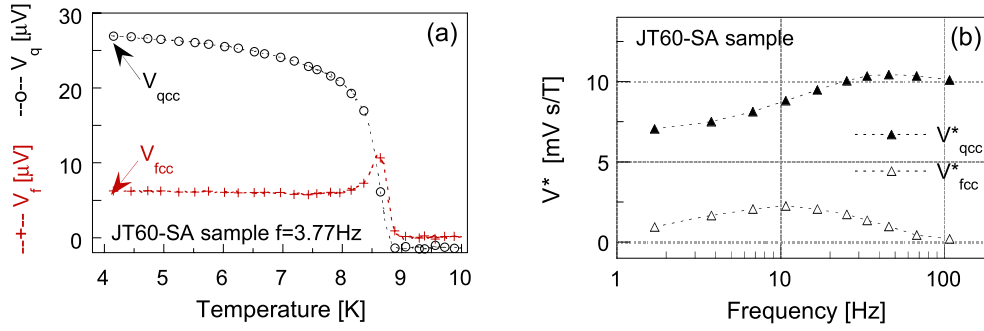
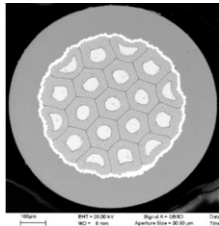
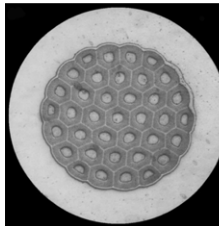
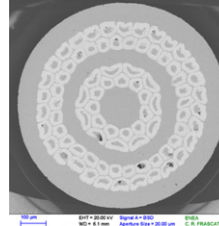
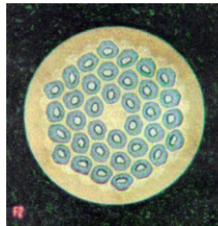


Figure 3. (a) The in-phase and out-of-phase signals measured by the lock-in, V_q and V_f , as a function of the temperature for JT60-SA strand $h = 0.94$ mm. V_{qcc} and V_{fcc} are the V_q and V_f values at 4.0 K. (b) The normalized signals V_{qcc}^* and V_{fcc}^* as a function of the ac frequency, f .

Table 1. Nb_3Sn wire features used in the experiments.

Sample	OST-I	OKSC	OCSI	EM-LMI
				
Manufacturer	Oxford Superconducting Technology	Outokumpu Superconductors	Outokumpu Copper Superconductors Italy	Europa Metall, Italy
Technology	Internal tin	Internal tin	Internal tin	Internal tin
OD (mm)	0.81	0.81	0.81	0.81
No. filaments	151 \times 19 bundles	37 bundles	82 bundles	150 \times 36 bundles
Twist pitch (mm)	15	24	15	10
Barrier type	Ta	Ta	Nb	Nb and Ta

measured by the lock-in, V_q and V_f , are directly proportional to the components of the ac susceptibility (real part, χ' , and imaginary part, χ'' , respectively) through a constant including the geometrical factors of the pick-up coil. The V_f is physically related to the energy coupling loss. This energy per cycle and per unit volume, W , in a composite strand under a transverse sinusoidal field $B_{ac} = B_0 \sin(\omega t)$ of angular frequency $\omega = 2\pi f$ and peak value B_0 is [1]:

$$W = \chi_0 \frac{B_0^2}{\mu_0} \pi \frac{\omega \tau}{1 + \omega^2 \tau^2} \quad (1)$$

where χ_0 is the external susceptibility under the condition of perfect screening and μ_0 is the vacuum permeability. The characteristic time constant, τ , is directly proportional to the square of the twist pitch, and inversely proportional to the transverse resistivity:

$$\tau = \frac{\mu_0}{2\rho_{et}} \left(\frac{L}{2\pi} \right)^2. \quad (2)$$

This model is valid when the full saturation condition is fulfilled, thus the measurements were performed in the presence of a static magnetic field $B_{ext} = 0.2$ T, transverse to the filament direction. The complete V_q and V_f behavior

as a function of the temperature is shown in figure 3(a), where V_{qcc} and V_{fcc} are the values corresponding to the lowest temperature ($T = 4.2$ K in this case). Figure 3(b) shows $V_{qcc}^* = \frac{V_{qcc}}{B_0 f}$ and $V_{fcc}^* = \frac{V_{fcc}}{B_0 f}$ as a function of the ac frequency f , with $B_0 = 1$ mT.

As expected, there is a peak on the V_{fcc}^* curve at about 11 Hz, which, considering a nominal wire twist pitch of $L = 15$ mm, leads to a resistivity value of about $\rho_{et}^{mag} = (0.25 \pm 0.06)$ n Ω m

2.2. Ac susceptibility in Nb_3Sn wires

Our aim is to check if the same ac technique previously described for testing NbTi strands could be applied to wires having a more complex layout, such as the Nb_3Sn ones. Several Nb_3Sn strands were used to cross check the measurement of ρ_{et} performed with both methods. Two different configurations of Nb_3Sn s/c wires have been chosen. The first typology has a very compact and dense filament bundle geometry through the wire cross section, and a single anti-diffusion barrier around the filamentary region. In the second typology the bundles are more spaced and distributed barriers are present around each filament bundle. In table 1

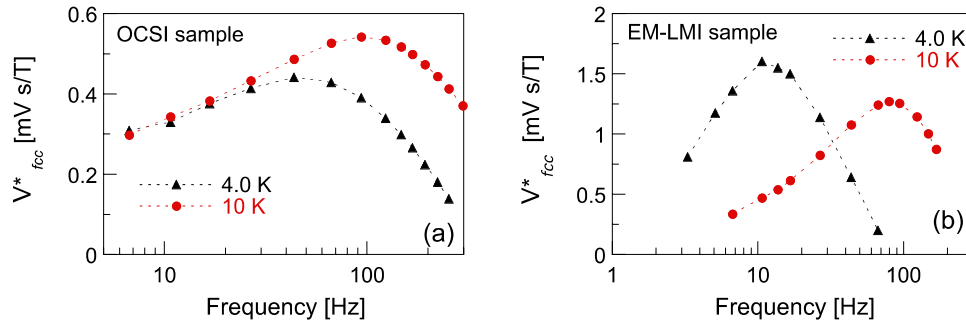


Figure 4. Measurement of V_{fcc}^* as a function of the frequency for OCSI wires (a), and measurement of V_{fcc}^* as a function of the frequency for EM-LMI wires (b).

Table 2. Transverse resistivity data—comparison between dc and ac methods.

Sample	f_0 @4.0 K (Hz)	ρ_{et}^{mag} @4.0 K (n Ω m)	ρ_{et}^{el} @4.2 K (n Ω m)	f_0 @10 K (Hz)	ρ_{et}^{mag} @10 K (n Ω m)	ρ_{et}^{el} @10 K (n Ω m)
OCSI	48 \pm 2	1.1 \pm 0.3	0.8 \pm 0.4	96 \pm 3	2.2 \pm 0.5	1.2 \pm 0.2
EM-LMI	11 \pm 1	0.11 \pm 0.03	0.26 \pm 0.08	80 \pm 3	0.8 \pm 0.2	1.4 \pm 0.2

the main features of the Nb₃Sn wires and their cross section images are reported. The samples OST-I and OKSC belong to the first typology of wires, OCSI and EM-LMI to the second typology. All the samples have been heat treated at ENEA laboratory, and each strand has been modeled into two shapes in order to obtain a suitable sample geometry for each kind of measurement: 3 mm long straight wire for dc resistance measurements, and a 2-turns coil shape, 5 mm wide, for ac measurements. This last geometry is necessary to have the sample length at least longer than one filament twist pitch.

Figures 4(a) and (b) show the measurement of V_{fcc}^* as a function of the frequency for OCSI and EM-LMI wires, respectively. The behavior of both samples is similar to the one observed on the NbTi strand, and the values of f_0 are reported in table 2. In contrast, for OST-I and OKSC strands, which belong to the first typology with a compact configuration of filament bundles surrounded by a single anti-diffusion barrier and a thick high purity copper ring outside, the dependence of V_{fcc}^* on the frequency is negligible. These results enforce the hypothesis of a relevant role for the strand layout.

Moreover, as often observed in Nb₃Sn wires [14], two superconducting phases are present, in OCSI and EM-LMI samples, one connected to Nb₃Sn, the other due to the presence of Nb (or Nb alloy). As a consequence, it is interesting to look for the characteristic frequency of such strands when the Nb is in the normal state. This condition is easily achieved by limiting the lowest temperature to 10 K when measuring V_{fcc}^* , and the corresponding curves are also shown in figures 4(a) and (b) for OCSI and EM-LMI wires, respectively.

The characteristic frequencies and the corresponding effective resistivities ρ_{et}^{mag} computed through formula (2), as well as the ρ_{et}^{el} values measured by electrical method, both at low temperature (4.0 K and 4.2 K, respectively) and at 10 K, are reported in table 2.

3. Discussion

There are obvious differences between the dc and ac measurements of the transverse resistivity. The first allows a direct measurement of the resistance, but the number of filaments involved in the current feeding is not well defined and a minimum size of 50 μ m in diameter is required for each bundle. Moreover the four-probe method is a local approach which, in complex strand layouts, could require many repeated measures at different locations, as the wire may include barriers among bundles or between the filamentary region and the Cu matrix.

The ac susceptibility is a global loss measurement due to the eddy currents, which are induced in all the filaments affected by the presence of the varying ac field. Though it may appear that the induced currents flow in the whole wire, we experienced that in presence of a compact layout (first typology of wires) the losses induced in the low-resistance outer copper ring prevail on the contribution due to the superconducting filamentary region, where a bronze matrix with an higher resistivity is present. Currents induced in the inner part of the strand are negligible, leading to a measure of the losses almost independent of the frequency. This occurrence made the measurement of the ac losses through the susceptibility inapplicable to OST-I and OKSC wires. Furthermore, to extract the resistivity value, the filament twist pitch is required. This parameter is estimated with a procedure affected by a high relative uncertainty (around 10%), which increases the error on the global measurement.

Finally, the direction of the external magnetic field ($B_{ext} = 0.2$ T) is parallel to the strand in the dc method and orthogonal in the ac technique. In spite of the various differences between the two approaches, the values of the transverse resistivity reported in table 2 show good compatibility.

In order to support the experimental results, indicating that the peak of the V_{fcc}^* occurs at a frequency corresponding

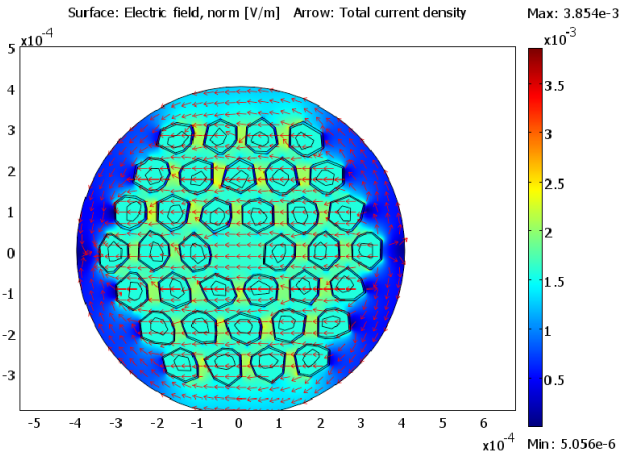


Figure 5. Current distribution for the EM-LMI strand computed in the case of a superconducting Nb barrier at 4.2 K.

to the characteristic time constant for the coupling current also in Nb₃Sn wires, we applied the same simple interpretative model as in NbTi wires, based on the work performed by Duchateau *et al* [15]. In order to calculate the transverse resistivity for the real wire, the actual layout rather than a crude approximation based on a simplified shell model has been considered.

The assumption is that the time scale of the varying field \dot{B} is much larger than the wire characteristic time T . Under this hypothesis the internal field is equal to the external field, and the voltage applied to a filament placed at a position (x, y) in the wire cross section is:

$$V(x) = \frac{\dot{B}}{2\pi} Lx. \quad (3)$$

Here the \dot{B} field is directed along the x direction (see figure 5 for the model cross section considered). We can find the correct current distribution by applying this condition to the filaments and solving the static electric problem governed by the Laplace equation. This should be done for the whole wire cross section. Actually, we cannot model thousands of filaments, but we can consider the large bundles of filament and apply the conditions directly to the bundles. This approximation would be reasonable, the filaments being in bundles surrounded by resistive anti-diffusion barriers, so that the coupling currents flow mainly through the parts of the Cu matrix surrounding the bundles. In figure 5 we show the geometry used for computation concerning the EM-LMI Nb₃Sn wire, the last one shown in table 1, i.e. one with multiple inter-diffusion barriers interposed around the bundles. It is worth noting the real bundle geometry has been considered to improve the model quality.

The area of each filament bundle is made by a Nb₃Sn ring surrounding a Sn core, having electrical resistivities of $\rho_{\text{Nb}_3\text{Sn}} = 1.0 \times 10^{-16} \Omega \text{ m}$ and $\rho_{\text{Sn}} = 1.7 \times 10^{-9} \Omega \text{ m}$, respectively. Around a single bundle there is an anti-diffusion barrier, made by a tantalum layer and an external Nb barrier, each one having a thickness of $3 \mu\text{m}$. Bundles are surrounded by the copper matrix, with resistivity (at $T = 4.2 \text{ K}$ and $B = 0.2 \text{ T}$) $\rho_{\text{Cu}} = 1.7 \times 10^{-10} \Omega \text{ m}$. The condition in

equation (3) is applied to the boundary of the filament bundles. The electrical problem has been solved using the ComsolTM finite elements code. With this approach we have $V_{x=0} = 0$. The obtained current distribution for the EM-LMI strand is shown in figure 5. We can see that the current paths include both the region external to the bundles and the inner core. By using the computed current distribution, we can calculate the electrical dissipation per unit volume by integrating the local calculated electric field $E(x, y)$ and the local current density $J(x, y)$ over the cross section and dividing by the whole cross section:

$$P = \frac{1}{S} \int_S E(x, y) J(x, y) dx dy. \quad (4)$$

Finally the time constant T is derived through [1]:

$$\tau = \frac{\mu_0 P}{2\dot{B}^2}. \quad (5)$$

Due to the presence of two superconducting phases (Nb and Nb₃Sn) the resulting time constant is computed for two different temperatures. At 4.2 K the Nb layer is superconducting, then a barrier resistivity $\rho_{\text{barr}} = 1.0 \times 10^{-11} \Omega \text{ m}$ is considered. In this case $\tau = 14 \text{ ms}$, corresponding to $f_0 = 11 \text{ Hz}$. Above 9 K a value of $\rho_{\text{barr}} = 1.0 \times 10^{-7} \Omega \text{ m}$ is used, the Nb being in the normal state, so obtaining $\tau = 2.2 \text{ ms}$ and $f_0 = 72 \text{ Hz}$. Those two characteristic frequencies computed so far are in very good agreement with the experimental ones.

4. Conclusions

In order to verify the possibility of applying the ac technique for contactless measurements of the transverse resistance on Nb₃Sn wires, we made an experimental comparison between the transverse resistivity values measured by a direct electrical method, $\rho_{\text{et}}^{\text{el}}$, and the results obtained with the ac inductive technique, $\rho_{\text{et}}^{\text{mag}}$.

The opportunity to compare the two methods was preliminarily validated on a NbTi strand, and a good compatibility between the results obtained with the two techniques was achieved. Then, two typologies of Nb₃Sn wires were considered: for the first, having a superconducting filamentary region surrounded by a single anti-diffusion barrier and a pure copper ring, the ac susceptibility approach could not be applied. For the second typology a convincing agreement has been achieved between the electrical and inductive methods, both at 4.2 and 10 K. In addition, a FEM simulation carried out on this latter typology (the LMI-EM strand) has supported the interpretation of the experimental results.

Further investigation will be carried out on samples belonging to the first typology in order to understand in more detail the effect of the outer copper ring as opposed to the bronze matrix of the filamentary zone.

Acknowledgments

The authors acknowledges A Ferrentino (University of Salerno) and R Viola (ENEA Frascati) for their invaluable technical support during the experiments.

References

- [1] Wilson M N 1983 *Superconducting Magnets* (Oxford: Oxford University Press)
- [2] Turck B, Wake M and Kobayashi M 1977 *Cryogenics* **17** 217
- [3] Kwasnitza K and Bruzzone P 1981 *Cryogenics* **21** 593
- [4] Holúbek T, Dhallé M and Kovác P 2007 *Supercond. Sci. Technol.* **20** 123
- [5] Fabbriatore P, Farinon S, Incardone S, Gambardella U, Saggese A and Volpini G 2009 *J. Appl. Phys.* **106** 083905
- [6] Corato V, Muzzi L, Besi Vetrella U and Della Corte A 2009 *J. Appl. Phys.* **105** 093930
- [7] Corato V, Muzzi L, Besi Vetrella U, Fiamozzi Zignani C and Della Corte A 2011 *IEEE Trans. Appl. Supercond.* **21** 3369
- [8] Zhou C *et al* 2013 *Supercond. Sci. Technol.* **26** 025002
- [9] Fabbriatore P *et al* 2008 *IEEE Trans. Appl. Supercond.* **18** 232
- [10] 2006 ITER Design Description Document: DDD 11; Magnet; Section 1: Engineering Description
- [11] Pizzuto A *et al* 2008 *IEEE Trans. Appl. Supercond.* **18** 505
- [12] Breschi M, Corato V, Fiamozzi Zignani C and Ribani P L 2011 *IEEE Trans. Appl. Supercond.* **21** 2372
- [13] Muzzi L, Affinito L, Corato V, De Marzi G, Di Zenobio A, Fiamozzi Zignani C, Napolitano M, Turtù S, Viola R and della Corte A 2009 *IEEE Trans. Appl. Supercond.* **19** 2544
- [14] Greco M, Bernini C, Fabbriatore P, Ferdeghini C, Gambardella U and Musenich R 2007 *IEEE Trans. Appl. Supercond.* **17** 2722
- [15] Duchateau L, Turck B and Ciazynski D 1998 *Handbook of Applied Superconductivity* ed B Seeber (Bristol: Institute of Physics Publishing) p 205